Solar-Assisted eBiorefinery

Photoelectrochemical Pairing of Oxyfunctionalization and Hydrogenation Reactions

Choi, Da Som; Kim, Jinhyun; Hollmann, Frank; Park, Chan Beum

DOI
10.1002/anie.202006893

Publication date
2020

Document Version
Final published version

Published in
Angewandte Chemie - International Edition

Photoelectrochemistry Hot Paper

How to cite:
International Edition: doi.org/10.1002/anie.202006893
German Edition: doi.org/10.1002/ange.202006893

Solar-Assisted eBiorefinery: Photoelectrochemical Pairing of Oxyfunctionalization and Hydrogenation Reactions

*Da Som Choi, Jinhyun Kim, Frank Hollmann, and Chan Beum Park**

Abstract: *Inspired by natural photosynthesis, biocatalytic photoelectrochemical (PEC) platforms are gaining prominence for the conversion of solar energy into useful chemicals by combining redox biocatalysis and photoelectrocatalysis. Herein, we report a dual biocatalytic PEC platform consisting of a molybdenum (Mo)-doped $BiVO_4$ (Mo:$BiVO_4$) photoanode and an inverse opal ITO (IO-ITO) cathode that gives rise to the coupling of peroxygenase and ene-reductase-mediated catalysis, respectively. In the PEC cell, the photoexcited electrons generated from the Mo:$BiVO_4$ are transferred to the IO-ITO and regenerate reduced flavin mononucleotides to drive ene-reductase-catalyzed trans-hydrogenation of ketoisophrone to (R)-levodione. Meanwhile, the photoactivated Mo:$BiVO_4$ evolves H_2O_2 in situ via a two-electron water-oxidation process with the aid of an applied bias, which simultaneously supplies peroxygenases to drive selective hydroxylation of ethylbenzene into enantiopure (R)-1-phenyl-1-hydroxyethane. Thus, the deliberate integration of PEC systems with redox biocatalytic reactions can simultaneously produce valuable chemicals on both electrodes using solar-powered electrons and water.*

Biocatalytic photoelectrochemical (PEC) platforms convert solar energy into fuels and value-added chemicals by mimicking natural photosynthesis.[1] In the PEC platforms, photoexcited charge carriers from photoelectrodes are transferred to the catalytic center of oxidoreductases either directly or indirectly and promote biocatalytic reactions.[2] Compared with homogeneous photocatalysis, biocatalytic PEC platforms can minimize back electron transfer and electron-hole recombination because of the configuration in which two electrodes are connected by an external wire.[3] Furthermore, spatial separation of anodic and cathodic reactions in a PEC platform avoids oxidation of reduced redox mediators or products at the anode. In addition, the Fermi level of electrons can be modulated by the external bias applied at the working electrode to drive a desired redox reaction selectively.[4] To date, most PEC-based biotransformations have been focused on driving cathodic reactions, whereas the anodic process has rarely been studied.

Herein, we pair enzymatic anodic and cathodic reactions in a PEC platform to achieve solar-assisted dual biotransformations. We constructed the PEC platform configured with a molybdenum (Mo)-doped bismuth vanadate (Mo:$BiVO_4$) photoanode and an inverse opal ITO (IO-ITO) electrode, as depicted in Scheme 1. For the biocatalytic reductive reaction, we chose the ene-reductase of the Old Yellow Enzyme family from *Thermus scotoductus* (*Ts*OYE). *Ts*OYEs catalyze the asymmetric *trans*-hydrogenation of conjugated C=C double bonds.[5] The costly NAD(P)H cofactor can be omitted by regenerating the enzymes directly via reduced FMN.[6] In the proposed PEC scheme, the hierarchically structured ITO electrodes reduce FMN redox mediators to promote the *Ts*OYE-catalyzed asymmetric reduction.

For the photoelectrochemical oxidation of water, we employed an n-type $BiVO_4$ photoanode because it exhibits promising selectivity toward two-electron water oxidation to generate hydrogen peroxide.[7] In addition, the monoclinic $BiVO_4$ has intrinsic advantages such as sufficient light absorption capacity due to its narrower band gap of 2.4 eV,[8] suitable valence band-edge positions,[9] and superior photostability in aqueous media.[10] To improve electrical properties and its activity in H_2O_2 production, we used hexavalent molybdenum as a metallic dopant for the $BiVO_4$ photoanode. In situ production of H_2O_2 on a Mo:$BiVO_4$ photoanode promotes peroxygenase-catalyzed, selective oxyfunctionalization reactions.[11] As a model biocatalyst, we used

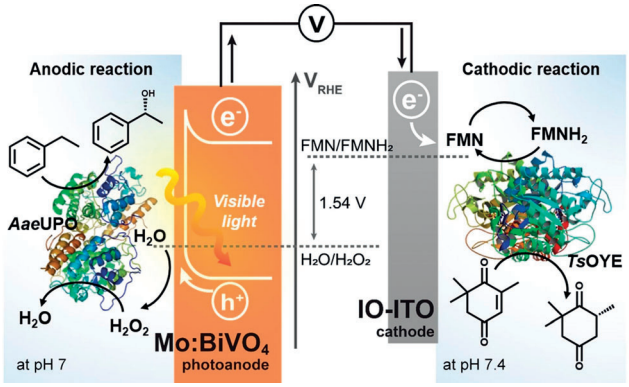

Scheme 1. Schematic illustration of solar-assisted photoelectrochemical cell for dual biotransformations. *Aae*UPO-mediated biotransformation is driven by in situ provision of H_2O_2 via two-electron water oxidation at the Mo:$BiVO_4$ photoanode under illumination. Simultaneously, the IO-ITO cathode reduces FMN mediators by delivering the photoexcited electrons from the Mo:$BiVO_4$ photoanode, and then facilitates the *Ts*OYE-catalyzed asymmetric reduction.

[*] D. S. Choi, J. Kim, Prof. Dr. C. B. Park
Department of Materials Science and Engineering
Korea Advanced Institute of Science and Technology
335 Science Road, Daejeon 34141 (Republic of Korea)
E-mail: parkcb@kaist.ac.kr
Prof. Dr. F. Hollmann
Department of Biotechnology, Delft University of Technology
Van der Maasweg 9, 2629HZ Delft (The Netherlands)
Supporting information and the ORCID identification number(s) for the author(s) of this article can be found under: https://doi.org/10.1002/anie.202006893.

the unspecific peroxygenase from *Agrocybe Aegerita* (*Aae*UPO) to drive enantioselective hydroxylation of ethylbenzene to (*R*)-1-phenyl-1-hydroxyethane.

We synthesized a high surface area IO-ITO electrode[12] as a cathode for electron transport to the FMN mediator. IO-ITO films were fabricated on an F-doped SnO_2 (FTO) substrate through a colloidal co-assembly process using ITO nanoparticles (< 50 nm diameter) and polystyrene spheres (800 nm diameter). After removal of the sacrificial polystyrene template, a mesoporous ITO framework is formed surrounding interconnected macroporous voids (Figure 1 a and Figure S1 in the Supporting Information). By controlling the amount of polystyrene-ITO dispersion cast on the FTO substrate, we were able to tune the thickness of the IO-ITO film approximately from 5 to 21 μm (Figure S2). We estimated the relative electrochemically active surface area (ECSA) of the flat ITO and IO-ITO electrodes by analyzing double layer capacitance (C_{dl}) using cyclic voltammetry (Figure 1 b).[13] The slope of the linear fit to non-Faradaic capacitive currents versus scan rate corresponded to the capacitance of electrodes. We found that the C_{dl} of IO-ITO electrodes increased from 1.77 to 5.73 mF cm^{-2} as the IO-ITO thickness increased. In contrast, the planar ITO electrode exhibited much lower C_{dl} value (0.02 mF cm^{-2}). Considering that C_{dl} is linearly proportional to the ECSA of materials with similar composition,[14] these results suggest that the IO structure provides a higher ECSA compared to that of the planar ITO.

We investigated charge transfer performance of IO-ITO electrodes by performing electrochemical impedance spectroscopy (EIS) measurements (Figure S3). EIS spectra were measured at −0.5 V (vs. Ag/AgCl) and plotted in the form of a Nyquist diagram over the frequency range of 0.1 to 10000 Hz for planar ITO and IO-ITO electrodes. We evaluated the charge transfer resistance of electrodes in terms of the semicircle diameter of the Nyquist plots at high frequencies. The IO-ITO electrode exhibited a much smaller arc than that of the planar ITO, which indicates that macroporous IO structure promotes efficient charge transfer at the electrode/electrolyte interface, hindering the charge recombination.[15]

To compare electrocatalytic characteristics of planar ITO and IO-ITO electrodes for the reduction of FMN, we carried out cyclic voltammetric analysis. As shown in Figure 1 c, the reduction peak current density of the IO-ITO electrode was −0.43 mA cm^{-2}, which was five times higher than that of the planar ITO, suggesting that the macroporous architecture facilitates instant diffusion of reactants to the electrode surface, which should lead to superior FMN reduction performance. We verified the reduction of FMN by the IO-ITO electrode using UV/Vis spectroscopy in a three-electrode configuration. At −0.5 V (vs. Ag/AgCl), two characteristic absorbance peaks of FMN at 370 and 440 nm decreased simultaneously, indicating the reduction of FMN to $FMNH_2$ by the IO-ITO cathode (Figure 1 d).[6c] On the other hand, the planar ITO showed a slight change in the absorption spectra of FMN (Figure S4), indicating that FMN reduction on the planar ITO cathode is limited due to the low ECSA. Taken together, these results show that the hierarchical porosity of the IO-ITO electrode contributes to the enhancement of the electrode performance for FMN reduction via increased effective surface area and improved charge transfer kinetics.

To probe the capability of the IO-ITO electrode to transfer electrons to *Ts*OYE via the electron mediator FMN, we observed chronoamperometric response of the IO-ITO electrode. As displayed in Figure S5, the cathodic current was enhanced as FMN and *Ts*OYE were sequentially added to the electrolyte, which indicates effective electron transfer from the IO-ITO electrode to *Ts*OYE via FMN. We further verified asymmetric reduction of ketoisophorone to (*R*)-levodione by *Ts*OYE using the IO-ITO cathode in a three-electrode configuration. The bioelectrocatalytic system yielded 3.29 mM of (*R*)-levodione (87 % *ee*) after 2 h (Figure S6). In the absence of either FMN or *Ts*OYE, no product formation was detected. Using a flat ITO, only 0.24 mM of (*R*)-levodione was produced, which was much lower than that of the IO-ITO. These data are in line with the results of electrochemical characterization of planar ITO and IO-ITO electrodes. In addition, we observed an increase in (*R*)-levodione production rate from 0.55 to 1.64 mM h^{-1} as the IO-ITO thickness increased (Figure S7), which suggests that increasing the ECSA of electrode enhanced the rate of electron transport to *Ts*OYE via FMN.

Next, we prepared a nanoporous $BiVO_4$ photoanode to drive photoelectrochemical in situ H_2O_2 generation from water oxidation under illumination. The BiOI film was electrodeposited on the FTO surface, then converted to $BiVO_4$ by calcination with vanadium precursor.[16] During annealing, the nanosheets of BiOI were transformed to

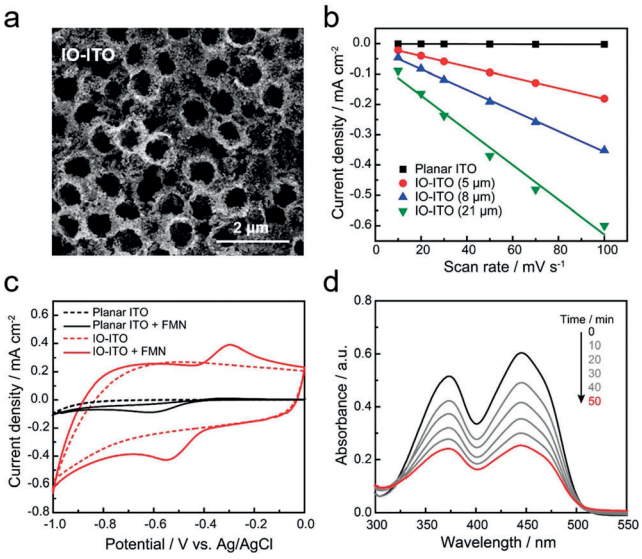

Figure 1. a) Top-view SEM image of IO-ITO electrode. b) Cathodic capacitive current densities of planar ITO and IO-ITO electrodes with varying thickness plotted against the scan rate. c) Cyclic voltammetry curves of planar ITO and IO-ITO electrodes before (dashed curve) and after addition of 20 mM FMN mediator (solid curve) at a scan rate of 50 mV s^{-1}. d) Changes in the UV/Vis absorbance spectra of 50 μM FMN in a 50 mM MOPS buffer (pH 7.4) by IO-ITO electrode at an applied bias of −0.5 V (vs. Ag/AgCl) under N_2. The geometrical surface area of all electrodes: 1 cm^2.

worm-like particles, resulting in the nanoporous $BiVO_4$ film with a band gap of 2.51 eV (Figure S8 and S9). To quantitatively evaluate the production of H_2O_2 on the $BiVO_4$ photoanode, we conducted a colorimetric assay of H_2O_2.[17] As shown in Figure 2a, H_2O_2 concentration increased linearly for over 60 min at 0.5 V (vs. Ag/AgCl) under illumination, whereas a negligible amount of H_2O_2 was detected in the absence of light, reflecting that H_2O_2 was generated via a photoelectrocatalytic water oxidation process. We further observed that the formation of H_2O_2 on the $BiVO_4$ photoanode under illumination enhanced continuously as the applied potential increased from 0.2 to 0.8 V (vs. Ag/AgCl) (Figure 2b).

To enhance the efficacy of the photoelectrocatalytic H_2O_2 generation on $BiVO_4$, we introduced a metallic dopant (Mo^{6+}) into the $BiVO_4$ film. Comparing the X-ray diffraction (XRD) patterns of Mo:$BiVO_4$ and pure $BiVO_4$ revealed that the scheelite-monoclinic phase of $BiVO_4$ was not changed by the Mo doping (Figure S10). EIS measurements on pure $BiVO_4$ and Mo:$BiVO_4$ showed that the charge transfer resistance at the electrode interface was reduced significantly with the increasing concentration of Mo dopant from 0 to 1.0% (Figure 2c and Figure S11). The result suggests that Mo facilitates charge transport at the electrode interface, eventually enhancing the activity of water oxidation. Furthermore, the photocurrent densities of the Mo:$BiVO_4$ photoanodes improved considerably across the entire potential range compared to the pure $BiVO_4$ photoanode (Figure S12). The enhanced photocurrent is ascribed to the improved electronic conductivity, which arises from the intrinsically enhanced charge carrier mobility and concentration resulting from the Mo doping.[18] A further increase in the dopant concentration (i.e., 5.0%), however, resulted in much higher interface resistance and lower photocurrent density, which is ascribed to unfavorable surface recombination due to the aggregation of excessive Mo.[19] We examined the effect of Mo doping on the photoelectrocatalytic H_2O_2 production (Figure 2d). In line with the improvements in the PEC performance, H_2O_2 production rate increased with the increase of Mo concentration from 0 to 1.0%. The 1.0% Mo:$BiVO_4$ photoanode exhibited the highest H_2O_2 formation rate of 38 $\mu M\,cm^{-2}\,min^{-1}$, which was 4.2 times higher than that of the pure $BiVO_4$ photoanode, whereas much slower oxidation of H_2O to H_2O_2 was observed for the 5.0% Mo:$BiVO_4$ photoanode. The faradaic efficiency (FE) of H_2O_2 generation reached a peak value of 52% in the 1.0% Mo:$BiVO_4$ photoanode, suggesting that the selectivity toward H_2O_2 is improved by the introduction of Mo. Taken together, the moderate Mo doping of $BiVO_4$ enhanced the activity of $BiVO_4$ toward H_2O_2 production due to the improved PEC properties.

Finally, we wired the 1.0% Mo:$BiVO_4$ photoanode to the IO-ITO cathode in a two-compartment setup connected by a salt bridge and investigated its photocurrent response using linear sweep voltammetry. Under illumination, a significantly enhanced photocurrent was obtained over the entire potential range (Figure S13a). From the J–V curve of the PEC system, we estimated the applied bias photon-to-current efficiency (ABPE, %) for the evolution of H_2O_2 and $FMNH_2$. ABPE values can be calculated using: $ABPE = J(V_{th} - V_{bias} - V_{chem})/P_{total}$, where J is the photocurrent density ($mA\,cm^{-2}$) under the applied bias voltage (V_{bias}), V_{th} (1.54 V) is the thermodynamic voltage determined by the difference between the redox potentials of H_2O/H_2O_2 (1.35 V vs. NHE) and FMN/$FMNH_2$ (−0.19 V vs. NHE), V_{chem} is the chemical bias between the two compartments (0.02 V), and P_{total} is the illumination power density ($100\,mW\,cm^{-2}$). The ABPE of whole PEC system reached 0.13% at an applied voltage of 0.86 V (Figure S13b).

To evaluate the performance of the 1.0% Mo:$BiVO_4$/IO-ITO system for paired bioelectrosynthesis, we measured the amount of products from each biocatalytic redox reaction by varying the applied bias from 0.5 to 1.0 V. Because the photovoltage (ca. 1.0 V)[20] generated from the Mo:$BiVO_4$ is smaller than the V_{th} for the overall reaction, at least 0.5 V of applied bias was required to drive biocatalytic reactions. As shown in Figure 3a, we observed a highly enantioselective conversion of ethylbenzene to (*R*)-1-phenyl-1-hydroxyethane (*ee* > 99%) regardless of the scale of applied bias. (*R*)-1-phenyl-1-hydroxyethane formation increased with the increasing applied voltage, and it reached the highest conversion rate of 0.51 $mM\,h^{-1}$ at 0.8 V. At more positive voltages, however, a decrease in product yield was observed. This decrease is attributed partly to the competition with one-electron water oxidation for OH· generation[21] and/or inactivation of the biocatalyst by OH· radicals,[22] limiting the overall efficiency. In particular, OH· radicals can oxidize the heme iron in the active site of peroxygenases, leading to their inactivation.[23] We expect that these issues associated with OH· radicals could be addressed by further optimization of $BiVO_4$ using different dopants[7c] or forming a heterojunc-

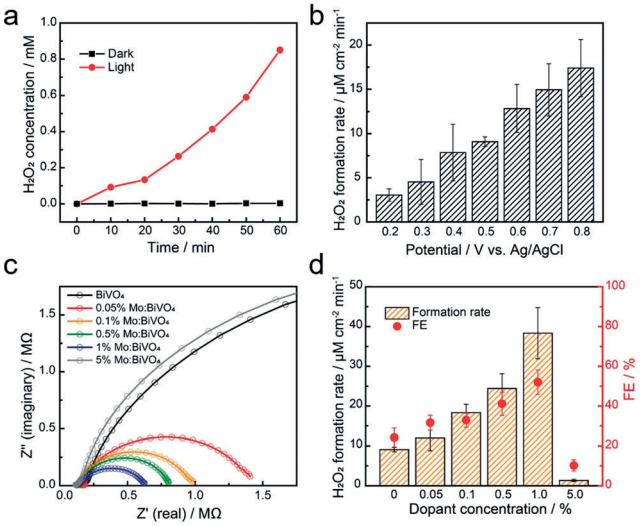

Figure 2. a) Time profiles of the generated H_2O_2 from pristine $BiVO_4$ photoanode at 0.5 V (vs. Ag/AgCl) in dark and under visible light illumination. b) H_2O_2 generation rates of $BiVO_4$ photoanodes as a function of applied potential under illumination. c) Nyquist plots of $BiVO_4$ and Mo:$BiVO_4$ electrodes (0.05%, 0.1%, 0.5%, 1%, and 5% concentration of Mo) measured at 0.3 V (vs. Ag/AgCl) in a 0.1 M KPi buffer (pH 7) under 1 sun illumination. d) Effects of Mo doping on formation rates of H_2O_2 and corresponding FEs for $BiVO_4$ photoanode. The geometrical surface areas of all electrodes: 1.5 cm^2.

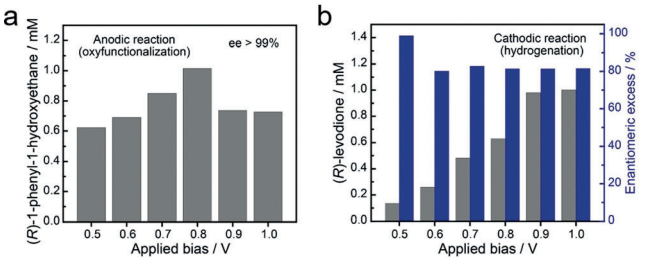

Figure 3. a) (*R*)-1-phenyl-1-hydroxyethane formation at the 1.0% Mo:$BiVO_4$ photoanode as a function of applied bias for 2 h. b) (*R*)-levodione formation and optical purity at the IO-ITO cathode as a function of applied bias for 2 h. The geometrical surface areas of the Mo:$BiVO_4$ and IO-ITO: 1.5 and 1 cm^2, respectively.

tion[24] for two-electron water oxidation reaction and by physical separation of *Aae*UPO from the photoelectrode.[25] In contrast, the generation of (*R*)-levodione by *Ts*OYE enhanced with the increasing applied bias (Figure 3b). At 1.0 V, the maximum conversion rate of 0.5 mM h^{-1} was observed with 82% *ee*. The relatively low optical purity of the product is attributed to non-enzymatic racemization of (*R*)-levodione.[26] At an applied bias above 0.9 V, only a slight increase in yield was observed in a similar trend to ABPE, indicating inefficient energy transfer at the high voltage.[27]

The biocatalytic PEC system requires an applied bias of at least 0.8 V to drive the complete reaction with an optimized conversion rate. Future research will address limitations associated with water oxidation for H_2O_2 generation and the requirement of an external applied bias. For example, a PEC system with a dual band gap configuration by coupling a $BiVO_4$-based photoanode with a suitable semiconductor (or photovoltaic) could reduce the additional bias to drive biocatalytic reactions by enhanced light harvesting with complementary light absorption.[28] We believe that the scope of our approach can be expanded to other redox enzymatic reactions through the regeneration of nicotinamide cofactors [i.e., NAD(P)H] on the cathode.[29] Numerous oxidoreductases in nature catalyze redox reactions using NAD(P)H as a hydride source.[30] Overall, the proof of concept presented herein provides a design strategy for solar-assisted eBiorefinery that can produce value-added chemicals on both electrodes simultaneously.

Acknowledgements

This study was supported by the National Research Foundation via the Creative Research Initiative Center (Grant number: NRF-2015R1A3A2066191), Republic of Korea.

Conflict of interest

The authors declare no conflict of interest.

Keywords: eBiorefinery · photobiocatalysis · photoelectrochemistry · photosynthesis · redox biocatalysis

[1] a) S. H. Lee, D. S. Choi, S. K. Kuk, C. B. Park, *Angew. Chem. Int. Ed.* **2018**, *57*, 7958 – 7985; *Angew. Chem.* **2018**, *130*, 8086 – 8116; b) L. Schmermund, V. Jurkaš, F. F. Özgen, G. D. Barone, H. C. Büchsenschütz, C. K. Winkler, S. Schmidt, R. Kourist, W. Kroutil, *ACS Catal.* **2019**, *9*, 4115 – 4144.
[2] J. Kim, C. B. Park, *Curr. Opin. Chem. Biol.* **2019**, *49*, 122 – 129.
[3] S. H. Lee, J. H. Kim, C. B. Park, *Chem. Eur. J.* **2013**, *19*, 4392 – 4406.
[4] J. Li, N. Wu, *Catal. Sci. Technol.* **2015**, *5*, 1360 – 1384.
[5] H. S. Toogood, N. S. Scrutton, *ACS Catal.* **2018**, *8*, 3532 – 3549.
[6] a) M. Mifsud, S. Gargiulo, S. Iborra, I. W. C. E. Arends, F. Hollmann, A. Corma, *Nat. Commun.* **2014**, *5*, 3145; b) S. H. Lee, D. S. Choi, M. Pesic, Y. W. Lee, C. E. Paul, F. Hollmann, C. B. Park, *Angew. Chem. Int. Ed.* **2017**, *56*, 8681 – 8685; *Angew. Chem.* **2017**, *129*, 8807 – 8811; c) E. J. Son, S. H. Lee, S. K. Kuk, M. Pesic, D. S. Choi, J. W. Ko, K. Kim, F. Hollmann, C. B. Park, *Adv. Funct. Mater.* **2018**, *28*, 1705232.
[7] a) K. Fuku, Y. Miyase, Y. Miseki, T. Gunji, K. Sayama, *ChemistrySelect* **2016**, *1*, 5721 – 5726; b) X. Shi, S. Siahrostami, G.-L. Li, Y. Zhang, P. Chakthranont, F. Studt, T. F. Jaramillo, X. Zheng, J. K. Nørskov, *Nat. Commun.* **2017**, *8*, 701; c) J. H. Baek, T. M. Gill, H. Abroshan, S. Park, X. Shi, J. Nørskov, H. S. Jung, S. Siahrostami, X. Zheng, *ACS Energy Lett.* **2019**, *4*, 720 – 728.
[8] D. Kang, T. W. Kim, S. R. Kubota, A. C. Cardiel, H. G. Cha, K.-S. Choi, *Chem. Rev.* **2015**, *115*, 12839 – 12887.
[9] J. K. Cooper, S. Gul, F. M. Toma, L. Chen, P.-A. Glans, J. Guo, J. W. Ager, J. Yano, I. D. Sharp, *Chem. Mater.* **2014**, *26*, 5365 – 5373.
[10] D. K. Lee, K.-S. Choi, *Nat. Energy* **2018**, *3*, 53 – 60.
[11] J. Dong, E. Fernández-Fueyo, F. Hollmann, C. E. Paul, M. Pesic, S. Schmidt, Y. Wang, S. Younes, W. Zhang, *Angew. Chem. Int. Ed.* **2018**, *57*, 9238 – 9261; *Angew. Chem.* **2018**, *130*, 9380 – 9404.
[12] D. Mersch, C.-Y. Lee, J. Z. Zhang, K. Brinkert, J. C. Fontecilla-Camps, A. W. Rutherford, E. Reisner, *J. Am. Chem. Soc.* **2015**, *137*, 8541 – 8549.
[13] Y. Yoon, A. S. Hall, Y. Surendranath, *Angew. Chem. Int. Ed.* **2016**, *55*, 15282 – 15286; *Angew. Chem.* **2016**, *128*, 15508 – 15512.
[14] J. Su, Y. Yang, G. Xia, J. Chen, P. Jiang, Q. Chen, *Nat. Commun.* **2017**, *8*, 14969.
[15] J. E. Park, S. Kim, O.-H. Kim, C.-Y. Ahn, M.-J. Kim, S. Y. Kang, T. I. Jeon, J.-G. Shim, D. W. Lee, J. H. Lee, Y.-H. Cho, Y.-E. Sung, *Nano Energy* **2019**, *58*, 158 – 166.
[16] T. W. Kim, K.-S. Choi, *Science* **2014**, *343*, 990 – 994.
[17] Y. Zhang, S. Tsitkov, H. Hess, *Nat. Commun.* **2016**, *7*, 13982.
[18] M. Zhou, J. Bao, Y. Xu, J. Zhang, J. Xie, M. Guan, C. Wang, L. Wen, Y. Lei, Y. Xie, *ACS Nano* **2014**, *8*, 7088 – 7098.
[19] a) Y. Park, D. Kang, K. S. Choi, *Phys. Chem. Chem. Phys.* **2014**, *16*, 1238 – 1246; b) M. Huang, J. Bian, W. Xiong, C. Huang, R. Zhang, *J. Mater. Chem. A* **2018**, *6*, 3602 – 3609.
[20] J. H. Kim, J. S. Lee, *Adv. Mater.* **2019**, *31*, 1806938.
[21] X. Shi, Y. Zhang, S. Siahrostami, X. Zheng, *Adv. Energy Mater.* **2018**, *8*, 1801158.
[22] W. Zhang, E. Fernández-Fueyo, Y. Ni, M. van Schie, J. Gacs, R. Renirie, R. Wever, F. G. Mutti, D. Rother, M. Alcalde, F. Hollmann, *Nat. Catal.* **2018**, *1*, 55 – 62.
[23] B. O. Burek, S. R. de Boer, F. Tieves, W. Zhang, M. van Schie, S. Bormann, M. Alcalde, D. Holtmann, F. Hollmann, D. W. Bahnemann, J. Z. Bloh, *ChemCatChem* **2019**, *11*, 3093 – 3100.
[24] Y. Miyase, S. Takasugi, S. Iguchi, Y. Miseki, T. Gunji, K. Sasaki, E. Fujita, K. Sayama, *Sustainable Energy Fuels* **2018**, *2*, 1621 – 1629.
[25] a) M. M. C. H. van Schie, W. Zhang, F. Tieves, D. S. Choi, C. B. Park, B. O. Burek, J. Z. Bloh, I. W. C. E. Arends, C. E. Paul, M. Alcalde, F. Hollmann, *ACS Catal.* **2019**, *9*, 7409 – 7417; b) J. Yoon, J. Kim, F. Tieves, W. Zhang, M. Alcalde, F. Hollmann, C. B. Park, *ACS Catal.* **2020**, *10*, 5236 – 5242.

[26] M. K. Peers, H. S. Toogood, D. J. Heyes, D. Mansell, B. J. Coe, N. S. Scrutton, *Catal. Sci. Technol.* **2016**, *6*, 169 – 177.
[27] S. K. Kuk, R. K. Singh, D. H. Nam, R. Singh, J.-K. Lee, C. B. Park, *Angew. Chem. Int. Ed.* **2017**, *56*, 3827 – 3832; *Angew. Chem.* **2017**, *129*, 3885 – 3890.
[28] a) Y. W. Lee, P. Boonmongkolras, E. J. Son, J. Kim, S. H. Lee, S. K. Kuk, J. W. Ko, B. Shin, C. B. Park, *Nat. Commun.* **2018**, *9*, 4208; b) S. K. Kuk, Y. Ham, K. Gopinath, P. Boonmongkolras, Y. Lee, Y. W. Lee, S. Kondaveeti, C. Ahn, B. Shin, J.-K. Lee, S. Jeon, C. B. Park, *Adv. Energy Mater.* **2019**, *9*, 1900029; c) D. S. Choi, H. Lee, F. Tieves, Y. W. Lee, E. J. Son, W. Zhang, B. Shin, F. Hollmann, C. B. Park, *ACS Catal.* **2019**, *9*, 10562 – 10566; d) S. K. Kuk, J. Jang, J. Kim, Y. Lee, Y. S. Kim, B. Koo, Y. W. Lee, J. W. Ko, B. Shin, J.-K. Lee, C. B. Park, *ChemSusChem* **2020**, *13*, 2940 – 2944.
[29] a) J. Kim, Y. W. Lee, E.-G. Choi, P. Boonmongkolras, B. W. Jeon, H. Lee, S. T. Kim, S. K. Kuk, Y. H. Kim, B. Shin, C. B. Park, *J. Mater. Chem. A* **2020**, *8*, 8496 – 8502; b) D. H. Nam, S. K. Kuk, H. Choe, S. Lee, J. W. Ko, E. J. Son, E.-G. Choi, Y. H. Kim, C. B. Park, *Green Chem.* **2016**, *18*, 5989 – 5993; c) D. H. Nam, G. M. Ryu, S. K. Kuk, D. S. Choi, E. J. Son, C. B. Park, *Appl. Catal. B* **2016**, *198*, 311 – 317; d) E. J. Son, J. W. Ko, S. K. Kuk, H. Choe, S. Lee, J. H. Kim, D. H. Nam, G. M. Ryu, Y. H. Kim, C. B. Park, *Chem. Commun.* **2016**, *52*, 9723 – 9726; e) W. S. Choi, S. H. Lee, J. W. Ko, C. B. Park, *ChemSusChem* **2016**, *9*, 1559 – 1564.
[30] X. Wang, T. Saba, H. H. P. Yiu, R. F. Howe, J. A. Anderson, J. Shi, *Chem* **2017**, *2*, 621 – 654.

Manuscript received: May 12, 2020
Version of record online: ■■ ■■, ■■■■

Communications

Photoelectrochemistry

D. S. Choi, J. Kim, F. Hollmann, C. B. Park* ——— ▮▮▮▮–▮▮▮▮

Solar-Assisted eBiorefinery: Photoelectrochemical Pairing of Oxyfunctionalization and Hydrogenation Reactions

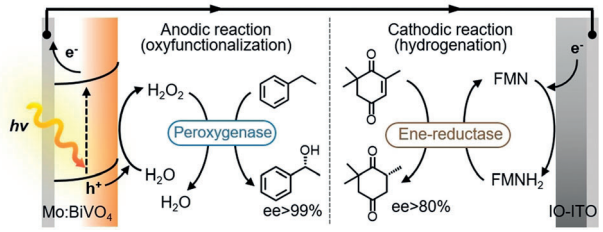

A biocatalytic photoelectrochemical platform for solar-assisted dual biotransformations is constructed by wiring a Mo-doped $BiVO_4$ photocathode and a hierarchical porous ITO electrode. The deliberate integration of enzymatic redox processes into the photoelectrochemical cell simultaneously facilitates peroxygenase- and ene-reductase-mediated enantioselective synthesis of high-value chemicals using solar-powered electrons and water.